Neuroscience Letters 651 (2017) 88–94

Contents lists available at ScienceDirect

Neuroscience Letters

journal homepage: www.elsevier.com/locate/neulet

Research article

A multilevel-ROI-features-based machine learning method for detection of morphometric biomarkers in Parkinson's disease

Bo Peng[a,b,c], Suhong Wang[d], Zhiyong Zhou[a], Yan Liu[a], Baotong Tong[a], Tao Zhang[c], Yakang Dai[a,*]

[a] Suzhou Institute of Biomedical Engineering and Technology, Chinese Academy of Sciences, Suzhou, Jiangsu 215163, China
[b] University of Chinese Academy of Sciences, Beijing 100049, China
[c] Changchun Institute of Optics, Fine Mechanics and Physics, Chinese Academy of Sciences, Changchun, Jilin 130033, China
[d] Department of Neuroscience, The Third Affiliated Hospital of Soochow University, Changzhou, Jiangsu 213003, China

HIGHLIGHTS

- We propose a machine learning method for detection of morphometric biomarkers in Parkinson's disease.
- The multilevel ROI features are constructed by using the low-level ROI features and the high-level correlative features.
- The classification performance of our method is improved compared with other methods using single-level features.
- The morphometric biomarkers that have been detected in our method are useful for assisted diagnosis of the disease.

ARTICLE INFO

Article history:
Received 1 March 2017
Received in revised form 7 April 2017
Accepted 18 April 2017
Available online 21 April 2017

Keywords:
multilevel ROI features
support vector machine (SVM)
magnetic resonance imaging (MRI)
Parkinson's disease

ABSTRACT

Machine learning methods have been widely used in recent years for detection of neuroimaging biomarkers in regions of interest (ROIs) and assisting diagnosis of neurodegenerative diseases. The innovation of this study is to use multilevel-ROI-features-based machine learning method to detect sensitive morphometric biomarkers in Parkinson's disease (PD). Specifically, the low-level ROI features (gray matter volume, cortical thickness, etc.) and high-level correlative features (connectivity between ROIs) are integrated to construct the multilevel ROI features. Filter- and wrapper- based feature selection method and multi-kernel support vector machine (SVM) are used in the classification algorithm. T1-weighted brain magnetic resonance (MR) images of 69 PD patients and 103 normal controls from the Parkinson's Progression Markers Initiative (PPMI) dataset are included in the study. The machine learning method performs well in classification between PD patients and normal controls with an accuracy of 85.78%, a specificity of 87.79%, and a sensitivity of 87.64%. The most sensitive biomarkers between PD patients and normal controls are mainly distributed in frontal lobe, parental lobe, limbic lobe, temporal lobe, and central region. The classification performance of our method with multilevel ROI features is significantly improved comparing with other classification methods using single-level features. The proposed method shows promising identification ability for detecting morphometric biomarkers in PD, thus confirming the potentiality of our method in assisting diagnosis of the disease.

1. Introduction

Parkinson's disease (PD) is one of the most common neurodegenerative diseases affecting middle-aged and elderly population all over the world [1]. The disease can be influenced by different factors, including social environment, use of medicine, and complication of neurological disease. The mechanism of PD is still unclear. The primary symptoms can be classified into motor symptoms and non-motor symptoms. Motor symptoms manifest as tremor, bradykinesia, rigidity muscles, and abnormal gait [2], whereas non-motor symptoms show mental disorders, sleep problems, autonomic dysfunction, and sensory disturbance [3]. How to assist diagnosis in the early stage of PD is a worldwide problem. Therefore, detecting morphometric biomarkers and developing identification technique for analysis of the disease are essential.

* Corresponding author.
E-mail address: daiyk@sibet.ac.cn (Y. Dai).

http://dx.doi.org/10.1016/j.neulet.2017.04.034
0304-3940/

At present, clinical diagnosis of PD is based on UK's National Institute for Health and Care Excellence (NICE) Parkinson's disease guideline [4], which is dependent on two or more motor symptoms, such as resting tremor, bradykinesia, or rigidity. However, the main symptoms of PD in evaluation of patients' conditions are similar to the symptoms that are caused by other factors, including progressive supranuclear palsy, multiple sclerosis, and Lowy's body dementia. In addition, dopamine levels of eighty percent corpus stratums have decreased when the patients are diagnosed with PD. These factors make it difficult for clinicians in early identification of the disease. Effective biomarkers that can reflect the patients' condition are needed urgently for analysis of the disease.

Neuroimaging technologies are widely used in diagnosis of neurodegenerative diseases. Magnetic resonance (MR) imaging is a neuroimaging technology that can provide precise information of brain structure and function with the advantage of imaging soft tissue in high resolution. In recent years, there has been a growing interest in using machine learning methods to detect neuroimaging biomarkers of regions of interest (ROIs). Studies show that machine-learning-based classification algorithms exhibit strong identification power on neurodegenerative disease, such as Huntington disease [5], Alzheimer's disease [6], and mild cognitive impairment [7]. In researches on PD, previous machine-learning-based studies reveal that the neuroimaging biomarkers that are related to PD mainly distribute in caudate nucleus [8], parahippocampal gyrus [9], and thalamus [10]. Machine learning methods can not only provide accurate biomarkers for better understanding of the disease but also provide an effective approach for assisting diagnosis of the disease. Nevertheless, existing methods for PD classification are mostly using single-level features (such as volumetric features or cortical features), which misses the high-level information of the brain.

The innovation of this study is to propose a multilevel-ROI-features-based machine learning method to detect morphometric biomarkers of PD on structural brain MR images. Specifically, we combine low-level ROI features (gray matter volume, cortical thickness, etc.) and high-level correlative features (connectivity between ROIs) to construct the multilevel ROI features, and use the filter- and wrapper- based features extraction approache and the multi-kernel support vector machine (SVM) for classification between PD patients and normal controls. The use of the low-level and the high-level features can integrate both structural information and brain connectivity for more accurate classification of PD. The validation of the classifier is performed on the Parkinson's Progression Markers Initiative (PPMI) dataset.

2. Materials and methods

2.1. Data

In this study, 69 PD patients and 103 normal controls from the Parkinson's Progression Markers Initiative (PPMI) dataset [11] are included. All participants have conducted neuropsychological tests, including Benton Judgment of Line Orientation, Total immediate recall (HVLT), Delayed recall (HVLT), Letter and number sequencing, Montreal Cognitive Assessment (MoCA) total score, Phonemic fluency, Semantic fluency, and Symbol Digit Modalities Test. All study procedures and ethical aspects were approved by the institutional review board. Written informed consents are obtained from all subjects.

The T1-weighted brain MR images are acquired by 3T SIMENS MEDICAL SYSTEM with the following parameters: repetition time (TR) = 2300 ms; echo time (TE) = 2.98 ms; flip angle (FA) = 9°; slice thickness = 1 mm; field of view (FOV) = 256 mm; matrix size = 240 × 256.

2.2. The multilevel-ROI-features-based machine learning method

The framework of the multilevel-ROI-features-based machine learning method is shown in Fig. 1. Before applying the machine learning method, all brain MR images are processed to extract the low-level ROI features and the high-level correlative features. Multilevel ROI features are constructed based on the low-level and high-level features. After that, feature extraction and feature selection are performed for the low-level and high-level features respectively. The kernel matrixes are constructed respectively for each feature type using radial basis function (RBF) kernel function before combining them into the final multi-kernel matrix.

2.2.1. Image processing

The original images are converted from DICOM format to ANALYZE format using the MRICron software (http://www.mccauslandcenter.sc.edu/mricro/mricron/). After that, the image processing procedures in BrainLab software [12] are performed, including five steps: (1) Image preprocessing: The input images are resampled and reoriented to standardize format. Then the N3 algorithm is used to correct the intensity of the images. (2) Brain extraction: Scalp, skull, and dura are removed as well as the non-brain tissues [13]. (3) Tissue segmentation: gray matter (GM), white matter (WM), and cerebrospinal fluid (CSF) are separated respectively [14]. (4) Brain label: The tissue segmented images are nonlinearly registered to the brain atlas. (5) Cortical surface reconstruction: The inner, middle, and outer surfaces of the cortex are reconstructed [15]. An anatomical parcellation of the Montreal Neurological Institute (MNI) based Automated Anatomical Labeling (AAL) template is used [16]. Because we focused on cortical gray matter regions, 12 subcortical ROIs are ignored [17]. After the whole processing, the morphometric measurements of GM volume, WM volume, CSF volume, cortical thickness, and cortical surface area of each ROI are obtained for all subjects.

2.2.2. Feature extraction

The low-level ROI features and the high-level correlative features are used to construct the multilevel ROI features. (1) The low-level ROI features that are extracted from the brain MR images using BrainLab software include GM volume, WM volume, CSF volume, cortical thickness, and cortical surface area. In order to decrease individual differences, the volumetric measurements of each ROI are normalized by dividing the intracranial volume of the subject. As for the cortical measurements, the cortical thicknesses of each ROI are normalized by dividing the respective standard deviation, and the cortical surface areas are normalized by dividing the total surface area of the brain. (2) The high-level correlative features are constructed by computing the correlation index of cortical thickness values between ROIs. A 78 × 78 correlative matrix is obtained for each subject, which conveys information of structural connectivity of the brain. Specifically, the correlation index between i-th and j-th ROI is defined as

$$c(i,j) = \exp\left\{-\frac{[t(i)-t(j)]^2}{2\left(\sigma_i{}^2+\sigma_j{}^2\right)}\right\} \quad (1)$$

where $t(i)$ and $t(j)$ denote cortical thickness value of the i-th and j-th ROI, and σ_i and σ_j denote the standard deviation of cortical thickness of the i-th and j-th ROI. Only 3003 elements $(N \times (N-1)/2)$, with $N = 78$) in the upper triangle of the correlative matrix are used on account of the similarity of the matrix.

2.2.3. Feature selection

In our method, mixed feature selection method is used to reduce the feature dimension, including filter-based approach and

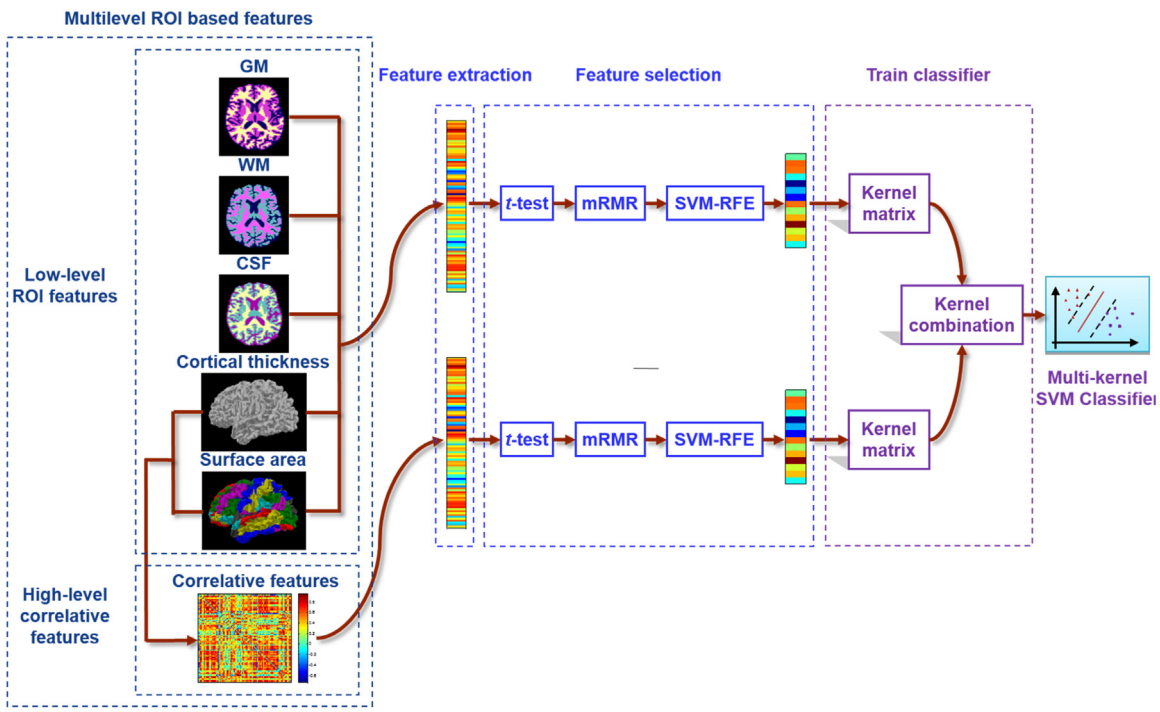

Fig. 1. Framework of the multilevel-ROI-features-based classification method.

wrapper-based approach. The dimension of the original ROI features is 390 (78 GM volume, 78 WM volume, 78 CSF volume, 78 cortical thickness, and 78 cortical surface area). The dimensionality of the original correlative feature is 3003 (upper triangular matrix of the 78 × 78 correlative matrix). The mixed feature selection method is used on each feature type respectively. First, *t*-test is used to choose the features whose *p* values are smaller than the threshold ($p < 0.05$). Then, the minimum redundancy and maximum relevance (mRMR) approach [18] is employed to further reduce the dimension of features. After these two steps, 30 features are retained for each feature type. Finally, a SVM based recursive feature elimination (SVM-RFE) method [19] is adopted to select the optimal features that are used to construct the classifier. Finally, 15 features are selected as the discriminative features for each feature type respectively. In order to ensure that the low-level ROI features and the high-level correlative features are within the same scale, all features are scaled to range [−1,1] before performing feature selection.

2.2.4. Classification algorithm

Because two types of features are included in our study: low-level ROI features and high-level correlative features, multi-kernel SVM is used to integrate these two types of featuresand provide a more comprehensive way of characterizing the whole feature space. Before we integrate these two types of features together, we first construct a single kernel matrix for each feature type respectively using radial basis function (RBF) kernel function. Suppose that we have N training samples $x_n^{(m)} \in R$, $n = 1, \ldots, N$, $m = 1, \ldots, M$ with M types of features and the corresponding labels $y_n \in \{-1, 1\}$. The purpose of the multi-SVM classifier is to estimate the decision function for a new test sample $\left(x^{(m)}, y\right)$. The decision function $F(x)$ is defined as

$$F(x) = sign\left(\sum_{n=1}^{N} \alpha_n y_n \sum_{m=1}^{M} \beta_m \left(x_n^{(m)}, x^{(m)}\right)\right) \quad (2)$$

where N is the number of samples; M is the number of feature types; $\beta_m > 0$ is the weighting factor of the M types of features; α_n is defined as $\sum_{n=1}^{N} \alpha_n y_n = 0$ with $0 \le \alpha_n \le C$, $n = 1, \ldots, N$ and C is the model parameter that controls the amount of constraint violations. In this way, the multi-kernel SVM classifier is able to determine that the new test sample is belonging to one or the other of the binary labeled training class (PD patient verses normal control).

2.3. Validation of the classifier

In our experiment, we randomly divided the whole data into two sets with similar number of subjects from each class in each set: one for training and the other one for testing. Two layer nested crossvalidation is employed to validate the classification algorithm. The aim of the inner crossvalidation is to determine the parameters that are used in construction of the classifier, while the outer cross-validation is used to evaluate the generalizability of the classifier on the testing set. This procedure is conducted using a 10-fold cross-validation. The classifier that performs best in the two layer nested cross-validation is considered to be the optimal classifier and the corresponding parameters will be used in the final SVM model to classify the new test sample.

3. Results

3.1. Demographic and clinical studies

Demographic and clinical information of PD patients and normal controls is listed in Table 1. Although no significant differences are found between the two groups in demographic information, PD patients are characterized by higher scores in clinical information, including Total immediate recall of Hopkins Verbal Learning Test (HVLT), Delayed recall of HVLT, Montreal Cognitive Assessment (MoCA) total score, Semantic fluency, and Symbol Digit Modalities Test.

Table 1
Demographic and clinical information of PD patients and normal controls.

	Normal controls(N = 103)	PD patients(N = 69)	Statistical test	*P* value
Variables				
Age, year, mean (SD)	60.57 (9.16)	59.78 (11.26)	t = 0.51	0.61
Female/male	32/71	25/44		
Education, year, mean (SD)	15.85 (2.71)	15.49 (3.05)	t = 0.82	0.42
Neuropsychological test results				
Benton Judgment of Line Orientation, mean (SD)	12.99 (2.02)	13.23 (1.78)	t = −0.81	0.42
Total immediate recall of HVLT, mean (SD)	24.24 (5.57)	26.20 (5.55)	t = −2.27	0.03
Delayed recall of HVLT, mean (SD)	8.49 (2.48)	9.25 (2.46)	t = −1.98	0.04
Letter and number sequencing, mean (SD)	10.19 (2.87)	10.78 (2.42)	t = −1.40	0.16
MoCA total score, mean (SD) (range)	27.35 (2.44)	28.03 (1.60)	t = −2.04	0.04
Phonemic fluency (MoCA), mean (SD)	13.70 (4.52)	14.88 (4.57)	t = −1.68	0.10
Semantic fluency, mean (SD)	51.31 (9.93)	55.72 (10.09)	t = −2.84	<0.01
Symbol Digit Modalities Test, mean (SD)	40.42 (11.21)	46.20 (8.39)	t = −3.65	<0.01

Abbreviations: N = number of participants; SD = standard deviation; PD = Parkinson's disease; HVLT = Hopkins Verbal Learning Test; MoCA = Movement Disorders Society. Comparisons between groups are performed using Student *t* test or χ^2 test. Significant at $p < 0.05$.

3.2. Classification performance

The multilevel ROI features are used in the classification framework, consisting of the low-level ROI features (GM volume, WM volume, CSF volume, combination of GM, WM, and CSF volume, cortical thickness, and cortical surface area) and the high-level correlative features. The classification performance is compared in Table 2 with the classification accuracy, area under receiver operating characteristic curve (AUC), sensitivity, specificity, Youden's index, *F*-score, Balanced Accuracy (BAC), and *p* values obtained from paired *t*-test on accuracy.

The classifier performs the worst among all feature types when using features of WM volume. For cortical thickness, the classification performance is significantly improved by using the high-level correlative feature comparing with the use of the low-level ROI features in cortical thickness, which indicates that the internal relationship between ROIs are reflected in the high-level correlative features. It is interesting to find that the combination of gray matter (GM), white matter (WM), and cerebrospinal fluid (CSF) volume performs similarly to the high-level correlative features. The multilevel ROI features perform the best in the classification with a relatively high accuracy of 85.78%. The statistically significant ($p < 0.0001$) results indicate that the multilevel ROI features are superior in characterizing the brain structural alterations and brain connections for PD patients. Moreover, the AUC, sensitivity, specificity, and other statistical evaluation measurements are also higher using the multilevel ROI features than using other features, which shows the potentiality of the classifier in classification between PD patients and normal controls.

3.3. The most sensitive features

TOP 15 of the most sensitive low-level ROI features and high-level correlative features are listed in Table 3. The sensitive low-level ROI features that include GM volume, WM volume, CSF volume, and cortical surface area are mainly distributed in both left and right hemisphere, which reveals the coordinative activities of the left and right brain. The low-level ROI features that are contributed the most in PD classification include frontal lobe (left orbitofrontal cortex (inferior), right middle frontal gyrus, left paracentral lobule, and left orbitofrontal cortex (medial)), parietal lobe (right supramarginal gyrus, left superior parietal gyrus, right angular gyrus, and left precuneus), central region (bilateral postcentral gyrus), occipital lobe (right fusiform gyrus), temporal lobe (right inferior temporal gyrus), and limbic lobe (left ParaHippocampal gyrus). Fig. 2(a) illustrates the most sensitive low-level ROI features that are mapping onto cortical surface.

The most sensitive high-level correlated features are drawn on the connection diagram (Fig. 2(b)), generating using an interrelationship displaying tool called Circos (www.cpan.org/ports) [20]. It can be found that pairs of ROIs (connected with smooth curve in the connection diagram) that are sensitive for PD classification are located in multiple lobes and both the left and right hemisphere, including left frontal lobe (left superior frontal gyrus (dorsal), left inferior frontal gyrus (triangular), left supplementary motor area, and left olfactory), right frontal lobe (right middle frontal gyrus, right orbitofrontal cortex (middle), right inferior frontal gyrus (opercular), right inferior frontal gyrus (triangular), right supplementary motor area, right superior frontal gyrus (medial), right orbitofrontal cortex (medial), and right rectus gyrus), left limbic lobe (left anterior cingulate gyrus and left ParaHippocampal gyrus), right limbic lobe (right temporal pole (superior)), left central region (left precentral gyrus), right central region (right rolandic operculum), right temporal lobe (right superior temporal gyrus and right middle temporal gyrus), and right Insula. It can be observed that most of the TOP 15 high-level correlated features are located in right frontal lobe with thicker and darker lines as shown in Fig. 2(b).

4. Discussion

Accurate and efficient PD classification with neuroimaging biomarkers has attracted intensive attention in recent years. So far, the biomarkers are based on either volumetric information [21] or cortical information [22,23]. It has been shown that these biomarkers are utilized in classification of PD patients from normal controls. However, these features cannot reflect synthesize information of the disease. For this reason, the multilevel ROI features that provide integrated information of the brain are essential for detecting PD-related morphometric biomarkers and increasing our understanding of the disease.

Machine learning methods have been widely used for identifying sensitive biomarkers in analysis of neurodegenerative diseases [24]. While most studies concentrate on measuring morphometric abnormalities in single ROIs, our study reveals that multilevel ROI features can be utilized to provide extra information at the whole brain level. In this study, we propose a multilevel-ROI-features-based machine learning method using multi-kernel SVM classifier. Improved classification performance is achieved using the PPMI dataset (accuracy = 85.78%, specificity = 87.79%, and sensitivity = 87.64%), which indicates the promising generalizability and identification power of our method to apply to similar problems. The proposed classification method is also compared with other approaches using PPMI dataset and SVM (Table 4). The classification accuracy is improved comparing with Chen's method [25].

Table 2
Classification performance using different feature types.

	Feature types							
	Low-level ROI features						High-level correlative features	Multilevel ROI features
Statisticalmeasures	GM	WM	CSF	GM + WM+CSF	Thickness	Area	Correlative	
ACC	65.2732	66.4250	66.7343	71.6133	68.2488	67.4469	73.6816	85.7816
AUC	0.6437	0.6497	0.6433	0.7556	0.6745	0.6541	0.8158	0.8363
SEN	0.6527	0.6640	0.6673	0.7056	0.6829	0.6747	0.7368	0.8764
SPE	0.6384	0.6482	0.6451	0.7263	0.6697	0.6508	0.7385	0.8779
Y	0.7604	0.7726	0.7834	0.8509	0.8002	0.7947	0.8475	0.8674
F	0.3426	0.3796	0.3841	0.4127	0.3982	0.3941	0.4529	0.6744
BAC	0.6763	0.6948	0.6803	0.7306	0.6913	0.6886	0.7557	0.8357
p value	<0.0001	<0.0001	<0.0001	<0.0001	<0.0001	<0.0001	<0.0001	–

Table 3
TOP 15 of the most sensitive low-level ROI features and high-level correlative features.

No.	Low-level ROI features	High-level correlative features
1	Orbitofrontal cortex (inferior)_L_C	Anterior cingulate gyrus_L – Superior temporal gyrus_R
2	Postcentral gyrus_R_C	Rolandic operculum_R – Supplementary motor area_L
3	Middle frontal gyrus_R_A	Supplementary motor area_R –Olfactory_L
4	Supramarginal gyrus_R_A	Superior frontal gyrus (dorsal)_L – Insula_R
5	Inferior temporal gyrus_R_W	ParaHippocampal gyrus_L – Middle temporal gyrus_R
6	Superior parietal gyrus_L_G	Supplementary motor area_R – Orbitofrontal cortex (medial)_R
7	Angular gyrus_R_A	Superior frontal gyrus (dorsal)_L – Supplementary motor area_L
8	Paracentral lobule_L_G	Olfactory_L – Rectus gyrus_R
9	Precuneus_L_A	Middle frontal gyrus_R – Inferior frontal gyrus (triangular)_R
10	Postcentral gyrus_L_A	Orbitofrontal cortex (middle)_R – Inferior frontal gyrus (opercular)_R
11	ParaHippocampal gyrus_L_G	Precentral gyrus_L – Orbitofrontal cortex (middle)_R
12	Fusiform gyrus_R_W	Superior frontal gyrus (dorsal)_L – Middle frontal gyrus_R
13	Orbitofrontal cortex (medial)_L_W	Precentral gyrus_L – Temporal pole (superior)_R
14	Middle frontal gyrus_R_W	Superior frontal gyrus (medial)_R – Rectus gyrus_R
15	Fusiform gyrus_R_A	Inferior frontal gyrus (triangular)_L – Rectus gyrus_R

*R = right, L = left, G = gray matter, W = white matter, C = cerebrospinal fluid, A = cortical surface area.

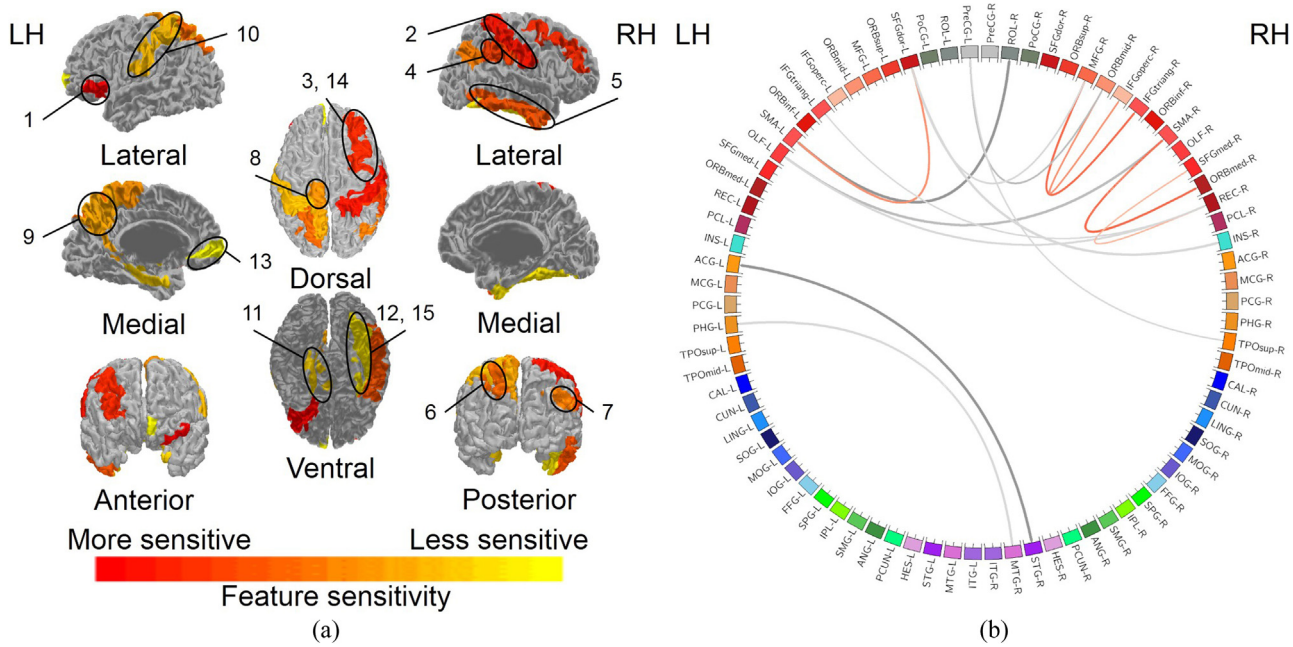

Fig. 2. Feature map of the most sensitive multilevel ROI features. (a) Low-level ROI features that are mapping onto cortical surface. (b) High-level correlative features. Red color lines indicate connections between ROIs in the same hemisphere, and gray color lines indicate connections between ROIs in the two sides of the brain. Thickness of each line reflects its selection frequency, e.g., thicker line indicates higher selection frequency. The labeled numbers on (a) are corresponding to the sequence numbers of the most sensitive ROI features in Table 3. (For interpretation of the references to colour in this figure legend, the reader is referred to the web version of this article.)

Although the classification accuracy of our method is similar to that of Salvatore's method [26], the specificity and sensitivity of our method are improved, which indicates that the multilevel ROI features have better ability in characterizing PD related brain morphometry.

The brain regions that are associated with PD pathology have already been reported in previous researches. These regions include

Table 4
Comparison with other approaches based on PPMI dataset.

	Chen [25]	Salvatore [26]	Our method
Dataset	PPMI	PPMI	PPMI
Sample number	18 PD patients 21 normal controls	28 PD patients 28 normal controls	69 PD patients103 normal controls
Data description	Brain MR images	Brain MR images	Brain MR images
Features	Scale invariant feature transform (SIFT) features	Principal Component Analysis (PCA) features	Multilevel ROI based features
Machine learning method	SVM	SVM	Multi-kernel SVM
Accuracy	80.0%	85.8%	85.8%
AUC	0.7800	–	0.8363
Specificity	–	86.0%	87.8%
Sensitivity	–	86.0%	87.6%

hippocampal [27], amygdalar [28], caudate [29], prefrontal cortex [30], and temporal lobe [31], most of which are also found in our results. The high-level correlated features are mainly located in the frontal lobe. It is interesting to find that there are more correlated features in the right hemisphere than in the left hemisphere. The right hemisphere has a special role in emotion regulation [32], which preliminarily shows the relationship between depression and structural connection in PD. Freezing of gait is a symptom of PD that is associated with dysfunction in processing cognitive information while walking [33]. Researchers find that structural connectiive abnormalities between different parts of the brain are one of the reasons for freezing of gait [34]. Our findings on brain connection are consistent with the previous studies, confirming the validity of the correlated features in our study.

Although most researches focus on morphometric features in single ROIs or distinct brain regions, our research shows that the multilevel ROI features integrating both structural information and brain connectivity can improve the classification performance between PD patients and normal controls. According to our results, PD-related abnormalities mainly locate at frontal lobe, parental lobe, limbic lobe, temporal lobe, and central region, which indicates that structural alterations are not located at specific regions but widespread over the whole brain. The proposed method can detect not only regions in low-level ROIs but also changes in high-level structural connections between ROIs. Since abnormalities generally appear in relevant brain regions, it is important to propose a method that can reflect the entire pattern of the alterations related to PD throughout the whole brain. The multilevel ROI features in our classification method convey synthetic and supplemental information, which provides a comprehensive approach for exploring the data of PD.

5. Conclusions

In this study, we propose a multilevel-ROI-features-based machine learning method using brain MR images to detect PD related morphometric biomarkers and improve the identification power of the disease. The low-level ROI features are extracted using BrainLab. Then the high-level correlated features are constructed by computing the similarity value of the cortical thickness between ROIs. The multilevel ROI features are integrated using both the low-level ROI features and the high-level correlative features. The classification performance of our method is improved by using our multilevel-ROI-features based classification method comparing with using other methods, which confirms the potentiality of the multilevel ROI features. The promising results demonstrate that our approach can provide comprehensive information that is useful for identification and analysis of PD and even for other neurodegenerative diseases.

Acknowledgements

This study is supported partly by the National 863 program of China (2015AA020514), NSFC grants (61501452), SSTP program (ZXY201426), Jiangsu Key Research and Development programs (BE2016613, BE2016010, BE2016010-3, BE2016010-4), postdoctoral research funding of Jiangsu province (1501089C), BKLN program, Suzhou scientific and technologic programs (ZXY201426, SYG201606, SZS201609), and SND medical plan project (2016Z010).

References

[1] T. Pringsheim, N. Jette, A. Frolkis, T.D. Steeves, The prevalence of Parkinson's disease: a systematic review and meta-analysis, Mov. Disord. 29 (13) (2014) 1583–1590.
[2] S.H. Fox, R. Katzenschlager, S.Y. Lim, B. Ravina, K. Seppi, M. Coelho, W. Poewe, O. Rascol, C.G. Goetz, C. Sampaio, The movement disorder society evidence-based medicine review update: treatments for the motor symptoms of Parkinson's disease, Mov. Disord. 26 (S3) (2011) S2–S41.
[3] K.R. Chaudhuri, A.H. Schapira, Non-motor symptoms of Parkinson's disease: dopaminergic pathophysiology and treatment, The Lancet Neurology 8 (5) (2009) 464–474.
[4] D.A. Stewart, NICE guideline for Parkinson's disease, Age Ageing 36 (3) (2007) 240–242.
[5] N.C. Reynolds, R.W. Prost, L.P. Mark, S.A. Joseph, MR-spectroscopic findings in juvenile-onset Huntington's disease, Mov. Disord. 23 (13) (2008) 1931–1935.
[6] S. Klöppel, C.M. Stonnington, C. Chu, B. Draganski, R.I. Scahill, J.D. Rohrer, N.C. Fox, C.R. Jack Jr., J. Ashburner, R.S. Frackowiak, Automatic classification of MR scans in Alzheimer's disease, Brain 131 (3) (2008) 681–689.
[7] S.J. Teipel, C. Born, M. Ewers, A.L. Bokde, M.F. Reiser, H.J. Möller, H. Hampel, Multivariate deformation-based analysis of brain atrophy to predict Alzheimer's disease in mild cognitive impairment, Neuroimage 38 (1) (2007) 13–24.
[8] O.P. Almeida, E.J. Burton, I. McKeith, A. Gholkar, D. Burn, J.T. O'Brien, MRI study of caudate nucleus volume in Parkinson's disease with and without dementia with Lewy bodies and Alzheimer's disease, Dement. Geriatr. Cogn. Disord. 16 (2) (2003) 57–63.
[9] B. Ramírez-Ruiz, M.J. Martí, E. Tolosa, D. Bartrés-Faz, C. Summerfield, P. Salgado-Pineda, B. Gómez-Ansón, C. Junqué, Longitudinal evaluation of cerebral morphological changes in Parkinson's disease with and without dementia, J. Neurol. 252 (11) (2005) 1345–1352.
[10] B.A. Pickut, W. Van Hecke, E. Kerckhofs, P. Mariën, S. Vanneste, P. Cras, P.M. Parizel, Mindfulness based intervention in Parkinson's disease leads to structural brain changes on MRI: a randomized controlled longitudinal trial, Clin. Neurol. Neurosurg. 115 (12) (2013) 2419–2425.
[11] K. Marek, D. Jennings, S. Lasch, A. Siderowf, C. Tanner, T. Simuni, et al., The parkinson progression marker initiative (PPMI), Prog. Neurobiol. 95 (4) (2011) 629–635.
[12] B. Peng, Z. Chen, L. Ma, Y. Dai, Cerebral alterations of type 2 diabetes mellitus on MRI: a pilot study, Neurosci. Lett. 606 (2015) 100–105.
[13] Y. Wang, G. Li, J. Nie, P.T. Yap, L. Guo, D. Shen, Consistent 4D brain extraction of serial brain MR images, SPIE Med. Imag. Int. Soc. Opt. Photon. 8669 (2013) (2013) 86693I.
[14] L. Wang, F. Shi, G. Li, D. Shen, 4D segmentation of brain MR images with constrained cortical thickness variation, PLoS One 8 (7) (2013) e64207.
[15] G. Li, J. Nie, G. Wu, Y. Wnag, D. Shen, Alzheimer's Disease Neuroimaging Initiative, Consistent reconstruction of cortical surfaces from longitudinal brain MR images, Neuroimage 59 (4) (2012) 3805–3820.
[16] N. Tzourio-Mazoyer, B. Landeau, D. Papathanassiou, F. Crivello, O. Etard, N. Delcroix, B. Mazoyer, M. Joliot, Automated anatomical labeling of activations in SPM using a macroscopic anatomical parcellation of the MNI MRI single-subject brain, Neuroimage 15 (1) (2002) 273–289.
[17] Y. Wang, J. Nie, P.T. Yap, G. Li, F. Shi, X. Geng, L. Guo, D. Shen, The Alzheimer's Disease Neuroimaging Initiative, Knowledge-guided robust MRI brain extraction for diverse large-scale neuroimaging studies on humans and non-human primates, PLoS One 9 (1) (2013) e77810.
[18] H. Peng, F. Long, C. Ding, Feature selection based on mutual information criteria of max-dependency, max-relevance, and min-redundancy, IEEE Trans. Pattern Anal. Mach. Intell. 27 (8) (2005) 1226–1238.

[19] K.B. Duan, J.C. Rajapakse, H. Wang, F. Azuaje, Multiple SVM-RFE for gene selection in cancer classification with expression data, IEEE Trans. Nanobiosci. 4 (3) (2005) 228–234.
[20] D. Holten, Hierarchical edge bundles: visualization of adjacency relations in hierarchical data, IEEE Trans. Vis. Comput. Graph. 12 (5) (2006) 741–748.
[21] T.R. Melzer, R. Watts, M.R. MacAskill, T.L. Pitcher, L. Livingston, R.J. Keenan, J.C. Dalrymple-Alford, T.J. Anderson, Grey matter atrophy in cognitively impaired Parkinson's disease, J. Neurol. Neurosurg. Psych. 83 (2) (2012) 188–194.
[22] T. Jubault, J.F. Gagnon, S. Karama, A. Ptito, A.L. Lafontaine, A.C. Evans, O. Monchi, Patterns of cortical thickness and surface area in early Parkinson's disease, Neuroimage 55 (2) (2011) 462–467.
[23] S.K. Song, J.E. Lee, H.J. Park, Y.H. Sohn, J.D. Lee, P.H. Lee, The pattern of cortical atrophy in patients with Parkinson's disease according to cognitive status, Mov. Disord. 26 (2) (2011) 289–296.
[24] J. Shi, X. Zheng, Y. Li, Q. Zhang, S. Ying, Multimodal neuroimaging feature learning with multimodal stacked deep polynomial networks for diagnosis of Alzheimer's disease, IEEE J. Biomed. Health. Inf. 99 (99) (2017) 1.
[25] Y. Chen, J. Storrs, L. Tan, L.J. Mazlack, J.H. Lee, L.J. Lu, Detecting brain structural changes as biomarker from magnetic resonance images using a local feature based SVM approach, J. Neurosci. Methods 221 (2014) 22–31.
[26] C. Salvatore, A. Cerasa, I. Castiglioni, F. Gallivanone, A. Augimeri, M. Lopez, M.C. Gilardi, A. Quattrone, Machine learning on brain MRI data for differential diagnosis of Parkinson's disease and Progressive Supranuclear Palsy, J. Neurosci. Methods 222 (2014) 230–237.
[27] P. Borghammer, K. Østergaard, P. Cumming, A. Gjedde, A. Rodell, N. Hall, M.M. Chakravarty, A deformation-based morphometry study of patients with early-stage Parkinson's disease, Eur. J. Neurol. 17 (2) (2010) 314–320.
[28] C. Junqué, B. Ramírez-Ruiz, E. Tolosa, C. Summerfield, M.J. Martí, P. Pastor, B. Gómez-Ansón, J.M. Mercader, Amygdalar and hippocampal MRI volumetric reductions in Parkinson's disease with dementia, Mov. Disord. 20 (5) (2005) 540–544.
[29] L.G. Apostolova, M. Beyer, A.E. Green, K.S. Hwang, J.H. Morra, Y.Y. Chou, C. Avedissian, D. Aarsland, C.C. Janvin, J.P. Larsen, J.L. Cummings, P.M. Thompson, Hippocampal, caudate, and ventricular changes in Parkinson's disease with and without dementia, Mov. Disord. 25 (6) (2010) 687–695.
[30] A.E. TAYLOR, J.A. Saint-Cyr, A.E. Lang, Frontal lobe dysfunction in Parkinson's disease, Brain 109 (5) (1986) 845–883.
[31] W.R. Martin, M. Wieler, M. Gee, R. Camicioli, Temporal lobe changes in early, untreated Parkinson's disease, Mov. Disord. 24 (13) (2009) 1949–1954.
[32] E.D. Ross, M.M. Mesulam, Dominant language functions of the right hemisphere? Prosody and emotional gesturing, Arch. Neurol. 36 (3) (1979) 144–148.
[33] J.M. Shine, E. Matar, P.B. Ward, S.J. Bolitho, M. Pearson, S.L. Naismith, S.J. Lewis, Differential neural activation patterns in patients with Parkinson's disease and freezing of gait in response to concurrent cognitive and motor load, PLoS One 8 (1) (2013) e52602.
[34] S. Vercruysse, I. Leunissen, G. Vervoort, W. Vandenberghe, S. Swinnen, A. Nieuwboer, Microstructural changes in white matter associated with freezing of gait in Parkinson's disease, Mov. Disord. 30 (4) (2015) 567–576.